Polymer Chemistry

Accepted Manuscript

ROYAL SOCIETY OF CHEMISTRY

www.rsc.org/polymers

Polymer Chemistry

PAPER

Influences of 2-(Diisopropylamino) Ethyl Methacrylate on Acid-Triggered Hydrolysis of Cyclic Benzylidene Acetals and Their Importance to Efficient of Drug Delivery

Received 00th January 20xx,
Accepted 00th January 20xx

DOI: 10.1039/x0xx00000x

www.rsc.org/

Minjie Tang[a], Zheng Yang[a], Zujian Feng[a], Junhui Zhou[a], Jinjian Liu[b], Jianfeng Liu[b], Weiwei Wang[c], Junqiang Zhao [a], Anjie Dong[a,d] and Liandong Deng[a†]

The ability to tune the degradation rate of biodegradable polymer, which can achieve precise spatiotemporal control of drug delivery, is of considerable interest for biomedical applications. In this study, a series of amphiphilic copolymers, methoxy poly(ethyleneglycol)-b-poly((2,4,6-Trimethoxybenzylidene-1,1,1-tris(hydroxymethyl) ethane methacrylate)-*co*-2-(diisopropylamino)ethyl methacrylate) (mPEG-b-P(TTMA-*co*-DPA), PETD) with different amount of DPA units, were synthesized by Reversible Addition Fragmentation Chain Transfer (RAFT) copolymerization, in which DPA containing tertiary amine were introduced to adjust the hydrolysis behavior of cyclic benzylidene acetals (CBAs). The molecular structure and chemical composition of PETD were characterized by ^{1}H NMR and gel permeation chromatography (GPC). PETD could self-assemble into stable nanoparticles with well-defined spherical morphology and displayed high drug loading capacity with doxorubicin (DOX) as the drug model. The hydrolysis behavior of CBAs in the PETD NPs was investigated by UV/vis spectroscopy under different pH values. Compared with PETD-0 bearing no DPA unit, the hydrolysis rate of PETD-3 with more DPA was faster, while PETD-1 with less DPA hydrolyzed much slower, which indicated that the introduction of DPA had an amphoteric effect on the hydrolysis behavior of CBAs under acid conditions. In addition, the in vitro release of DOX was also investigated under different pH conditions and the result was in accordance with the hydrolysis result. Furthermore, the results of fluorescence microscopy demonstrated improved internalization of DOX-loaded PETD-3 NPs in HepG-2 cells with rapid DOX release intracellularly, which showed considerable cytotoxicity against HepG-2 cells.

Introduction

pH-sensitive polymers are of interest in a variety of fields including nanoactuators, molecular switches, bimodal imaging, bioseparation microcantilever-based sensors, tissue engineering and drug delivery, etc.[1-6] Particularly, pH-sensitive drug delivery systems comprising polymer nanoparticles (NPs),[7] liposomes/polymersomes,[8,9] inorganic NPs,[10] star polymers,[11] dendrimers,[12] and layer-by-layer (LbL) assembled capsules[13] have attracted a surge of attentions, because the pH of most tumor tissues is mildly acidic and lower than that of normal tissues and the blood stream.[14-18] pH-sensitive amphiphilic polymers have been used to construct pH-triggerable delivery system by two major approaches. The first approach is to incorporate acid-labile bonds, such as hydrazine bond,[19] ortho-ester,[20,21] hydrazine,[22] oxime bonds,[23] cis-acotinyl[24] and acetal linkages[25-27] to facilitate the drug release in acidic endo/lysosomes. The second approach is to optimize the structure of polymers by incorporating different functional structures which can achieve the hydrophobic/hydrophilic transition and pH responsive dis-assembly or de-crosslinking to control drug release.[28-33]

Among these pH sensitive systems, acid-cleavable cyclic benzylidene acetals (CBAs) has been widely used in construction of pH sensitive delivery system[34-36] to enhance the drug loading, due to the π-π stacking interaction with drugs, such as paclitaxel, doxorubicin, camptothecin and curcumin.[37] However, hydrolysis rate of CBAs are relatively slower, resulting in unsatisfactory response rate to the acidic tumor microenvironment, compared with acyclic ketal.[38-40] Herein, we will report a novel method to enhance the pH responsiveness of CBAs based polymer to tumor acidic microenvironment by covalently incorporating ultrasensitive segments, 2-(diisopropylamino) ethyl methacrylate (DPA) bearing tertiary amino groups, which could be rapidly protonated under the endosomal pH,[41-43] and utilize CBAs based polymer to efficiently load doxorubicin for cancer therapy. The pH-sensitive amphiphilic copolymers, methoxy poly(ethylene glycol)-b-poly((2,4,6-Trimethoxybenzylidene-1,1,1-tris(hydroxymethyl) ethane methacrylate)-co-2-(diisopropylamino) ethyl methacrylate) (mPEG-b-P(TTMA-*co*-DPA), PETD), were synthesized by Reversible Addition

[a] Department of Polymer Science and Technology and Key Laboratory of Systems Bioengineering of the Ministry of Education, School of Chemical Engineering and Technology, Tianjin University, Tianjin 300072, China.
[b] Tianjin Key Laboratory of Molecular Nuclear Medicine, Institute of Radiation Medicine, Chinese Academy of Medical Science and Peking Union Medical College, Tianjin, China.
[c] Tianjin Key Laboratory of Biomaterial Research, Institute of Biomedical Engineering, Chinese Academy of Medical Science and Peking Union Medical College, Tianjin 300192, China.
[d] Collaborative Innovation Center of Chemical Science and Engineering (Tianjin), Tianjin 300072, China.
† Correspondin author. E-mail addresses: dengliandong@aliyun.com
Electronic Supplementary Information (ESI) available: [details of any supplementary information available should be included here]. See DOI: 10.1039/x0xx00000x

Fragmentation Chain Transfer (RAFT) copolymerization using $mPEG_{113}$-DTM as initiator as shown in Scheme 1. The structure and composition of polymer were characterized by ^1H NMR and gel permeation chromatography (GPC). The hydrolysis behavior of CBAs in the PETD NPs was investigated by UV/vis spectroscopy under different pH conditions. The self-assembly behaviors and *in vitro* release of DOX under different pH conditions were investigated. Besides, the cell uptake and cytotoxicity of DOX-loaded PETD NPs were also determined.

Experimental

Materials

2-(Dodecylthiocarbonothioylthio)-2-Methylpropionic acid (DTM) and 2, 4, 6-Trimethoxybenzylidene-1, 1, 1-tris (hydroxymethyl) ethane methacrylate (TTMA) were synthesized as reported previously.[34, 44] The structure were confirmed by ^{1}HNMR (Fig. S1- S2). Methoxy poly (ethylene glycol) (mPEG, Mn = 5000), 1,1,1-tris (hydroxymethyl) ethane (99%), 2,4,6-Trimethoxybenzaldehyde (98%), methacryloyl chloride (97%), 2-(diisopropylamino)ethyl methacrylate (97%), p-toluenesulfonic acid monohydrate (97%), n-dodecylthiol (99%) and carbon disulfide (99%) were used as received from Aldrich. Doxorubicin hydrochloride (DOX·HCl) was purchased from Zhejiang Hisun Pharmaceutical Co. Ltd. and was used as received. Tetrahydrofuran (THF), diethyl ether, ethyl acetate, dichloromethane (DCM), hexane, triethylamine, sodium hydride, and anhydrous magnesium sulfate were provided by Jiangtian Company (Tianjin, China). DCM, THF were dried under an argon atmosphere by refluxing over CaH_2 and distilled prior to use.

Synthesis and characterization of mPEG-DTM, mPEG-b-PTTMA and PETD

mPEG-DTM was synthesized by esterification reaction of the hydroxyl in mPEG and carboxyl in DTM. In brief, DCC (67.98 mg, 0.33 mmol) and DTM (54.75 mg, 0.15 mmol) were dissolved in dried DCM, then 4-(dimethylamino) pyridine (DMAP) (13.44 mg, 0.11 mmol) and mPEG (0.1 g, 0.1 mmol) was added into the mixture sequentially. Then the reaction was carried out at room temperature for 24 h. The reaction mixture was filtrated and then precipitated in cold diethyl ether. The product obtained was dried overnight in a vacuum oven at 25 °C with yield of 93.5%.

mPEG-b-PTTMA was synthesized by RAFT polymerization using mPEG-DTM as macromolecular chain transfer agent, AIBN as initiator. Briefly, mPEG-DTM (250mg), TTMA (233.3 mg), AIBN (3.85 mg) and THF (4 mL) were added into a 25 mL schlenk flask purged by three repeated vacuum/nitrogen cycles. After that, the flask was placed in a thermostatic oil bath at 70 °C for about 24 h under nitrogen atmosphere. PETD was synthesized under a condition similar to the synthesis of

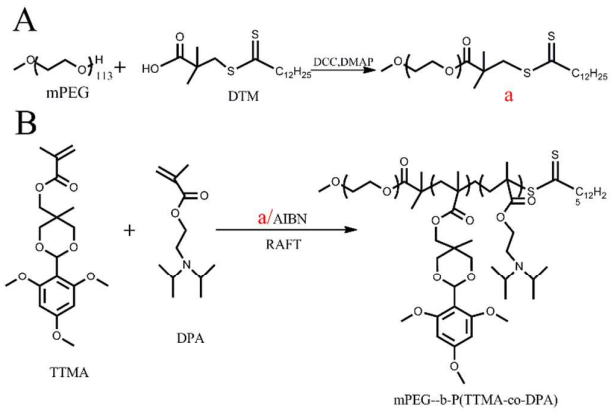

Scheme 1. Synthesis of mPEG-b-P(TTMA-co-DPA) via esterification reaction (A) and RAFT copolymerization (B).

mPEG-b-PTTMA, just substitute TTMA for the mixture of TTMA and DPA according to the different certain molar ratios.

The structure and composition of the polymers were characterized by ^{1}H NMR (Varian Unity-Plus INOVA 500) with $CDCl_3$ as a solvent and tetramethylsilane (TMS) as the internal standard. The molecular weight and molecular weight polydispersity index (Mw/Mn) of the copolymers and macroinitiator were measured by gel permeation chromatography (GPC, Waters Company, Milford, USA). THF was used as the eluting solvent with a flow rate of 1 mL/min and polystyrene was used as standard for calibration.

Preparation and Characterization of PETD NPs

The PETD NPs were prepared by the dialysis method. In brief, 1 mL DMSO containing 10 mg amphiphilic copolymer was dropwise added to 8 mL phosphate buffer (10 mM PB, pH 7.4) under stirring, which was followed by ultrasonication for 30 min. The solutions were dialyzed for 24 h in a dialysis bag with a molecular weight cut off (MWCO) of 3500 Da using PB (10 mM, pH 7.4) to remove the organic solvent. The size and size distribution (PDI) were measured using Dynamic laser scattering (DLS) measurements which were performed on a Brookhaven BI-200SM (Brookhaven Instruments Co., Holtsville, USA) at λ = 532 nm with a fixed detector angle of 90°. The morphology of the nanoparticles was determined by transmission electron microscopy (TEM, JEOL JEM-1011) with an accelerating voltage of 100 kV. The sample was prepared by adding a drop of NPs solution onto the copper grid and dried in air at room temperature before measurement.

Determination of Critical Micelle Concentration (CMC)

CMC was determined with steady-state fluorescence probe method using pyrene as the probe. The fluorescence spectra were recorded on a Varian fluorescence spectrophotometer at room temperature with the excitation wavelength of 373 nm. Sample solutions for fluorescence investigation were prepared as reported previously[33] and the concentrations ranged from 1.0×10^{-6} to 1.0 mg/mL. Sample solutions with various

concentrations were added to vials, sonicated for half an hour and equilibrated for 24 h at room temperature. The pyrene concentration in each vial was fixed at 6.0×10^{-7} mol/L. The CMC was obtained from the cross-point when extrapolating the intensity ratio I337/I330 at low and high concentration regions.

pH-Triggered hydrolysis of acetal groups

The acetal hydrolysis was followed using UV-visible spectrophotometer (TU-1900, China) to monitor the absorbance at 292 nm, according to the previous report.[34] The NPs solutions (0.1 wt%) were prepared and divided into three aliquots of 2 mL. Their pH were adjusted to 4.0, 5.0, and 7.4 by adding 50 μL of pH 4.0 acetate buffer, pH 5.0 acetate buffer and pH 7.4 PB buffer solution, respectively. The dispersions were shaken at 37 °C and 70 rpm. At the desired time intervals, 80 μL aliquot was taken out and diluted by adding 3.5 mL of PB (0.1 M, pH 7.4). The absorbance at 292 nm was observed. In the end, two drops of concentrated HCl were added to completely hydrolyze all the samples and they were measured again to determine the absorbance at 100% hydrolysis, which was used to calculate the degree of acetal hydrolysis.

DOX Loading and in vitro pH-Triggered DOX Release in the NPs

A solvent exchange method was used to prepare the DOX-loaded NPs. 1 mL of DMSO containing 10 mg amphiphilic copolymer and 1 mg DOX was dropwise added into 8 mL of PB (10 mM, pH 7.4) under stirring. After ultrasonication for 30 min and extensive dialysis (MWCO 3500) against PB (10 mM, pH 7.4) for 24 h to remove the organic solvent and free DOX, the DOX-loaded NPs solution was obtained. The entire process was carried out in the dark. To determine drug loading content (DLC) and drug loading efficiency (DLE), the DOX-loaded NPs solution was lyophilized and the freeze-dried DOX-loaded NPs were dissolved in DMSO and analyzed with UV/vis spectrophotometer at 425 nm. The standard curve was obtained with DOX/DMSO solutions with a series of DOX concentrations. DLC and DLE were calculated according to the following formulation:

$$\text{DLC (\%)} = \frac{\text{amount of loaded drug}}{\text{amount of drug–loaded nanoparticles}} \times 100\%$$

$$\text{DLE (\%)} = \frac{\text{amount of loaded drug}}{\text{total amount of drug in feed}} \times 100\%$$

To obtain the release profile of the DOX, three kinds of release media were chosed: (a) acetate buffer (10 mM, pH 4.0); (b) acetate buffer (10 mM, pH 5.0); (c) phosphate buffer (10 mM, pH 7.4). The DOX-loaded NPs were divided into three aliquots (each 5 mL). Their pH was adjusted to 4.0 or 5.0 using acetate buffer and to pH 7.4 using phosphate buffer. 5.0 mL of NPs solution (1.0 mg/mL) was added into a dialysis tube with a MWCO of 3.5 kDa. The dialysis tube was transferred into 20 mL of appropriate medium immediately and put into a shaker with 100 rmp at 37 °C. At predetermined time intervals, 5.0 mL of release medium was collected while an equivalent volume of fresh medium was added to guarantee the sink conditions. The concentration of DOX released was calculated according to the absorbance intensity at 500 nm with UV/vis spectroscopy. The release experiments at each time point were conducted in triplicate. The results presented are the average data with standard deviations.

Cell viability Assays

In vitro cytotoxicity of free DOX, blank PETD NPs and DOX-loaded NPs were studied by MTT assay against HepG-2 cells. All sample solutions were filtered with a 0.45 μm syringe filter and diluted into a series of concentrations with Dulbecco modified Eagle medium (DMEM). HepG-2 cells were seeded in 96-well plates at 1×10^4 cells per well in100.0 μL of complete Dulbecco modified Eagle medium (DMEM) and incubated at 37 °C in a 5% CO_2 atmosphere for 24 h. To determine the cytotoxicity of free DOX, blank and DOX-loaded NPs, the culture medium was replaced by 100 μL sample solutions at different concentrations (0~1.0 mg/mL) in DMEM. After 48 h incubation, the cells were treated by MTT asssy. The absorbance of MTT in each well was measured on Infinite M200 (TECAN, Mannedorf, Switzerland). The cell viability (%) was measured by comparing the absorbance at 540 nm with blank control wells containing only cell culture media. Triplicates were averaged as well as standard errors were calculated.

Cell Uptake Studies

For the determination of the cellular uptake of DOX, HepG-2 cells were seeded in a 6-well plate with a clean coverslip in each well and incubated up to the cell confluence of 60-80%. Thereafter, the cells were washed with PBS and incubated in a serum-free medium containing free DOX or DOX-loaded nanoparticles (DOX concentration 5 μg/mL) for 2 h and 4 h. After that, the cell monolayers were rinsed with 1 mL PBS (10 mM, pH 7.4) three times to remove excess nanoparticles or free DOX. For the cellular images, fresh PBS (10 mM, pH 7.4) was added to the plates and the cell images were visualized using a fluorescence microscope (Baxter, United States).

For flow cytometric analyses, HepG-2 cells were placed into 24-well plates (2×10^5 cells/well) and cultured in 2.0 mL of complete DMEM under a humidified atmosphere of 5% CO_2 and 95% air for 24 h at 37°C. The medium was then removed and culture media with free DOX and DOX-loaded NPs were changed at equivalent DOX concentration of 5.0 μg/mL. The cells were incubated for additional 2 and 4 h, followed by washing with 10 mM PB (pH 7.4) three times. The analysis was examined by flow cytometer on an FACS calibur flow cytometer (BD Biosciences US).

Results and discussion

Synthesis and Characterization of Copolymers

In this study, a series of copolymers (PETD-0,1,2,3) bearing TTMA and DPA with different feed ratios were obtained by RAFT copolymerization using $mPEG_{113}$-DTM as a macromolecular chain transfer agent (Fig. S3). The structure and chemical composition of the mPEG-PTTMA and mPEG-b-P (TTMA-co-DPA) were characterized by ^{1}H NMR (Fig.1). The sharp peaks at 3.35 ppm (a) and 3.65 ppm (b) were attributed to the methoxyl (terminal CH_3O-) and methylene protons (-OCH_2CH_2O-) of mPEG, respectively. The characteristic peaks of PTTMA were observed at 6.03 ppm (aromatic protons, n) and 5.83 ppm (Ar-CH-, l). The characteristic signals in PDPA at 2.86 ppm (-N-CH-, t) and 2.95 ppm (-CH_2-N-, q) were also obtained, indicating successful synthesis of the PETD copolymers. The molar ratio of DPA calculated by ^{1}H NMR was consistent with the designed value from 0 of PETD-0 to 25% of PETD-3 as

shown in Table 1. Furthermore, the narrow molecular weight distributions (Mw/Mn =1.21-1.27) determined by GPC were obtained for all PETDs (Figure S4). Also, the molecular weights calculated from ^{1}H NMR and obtained by GPC were both close to the theoretical values because of the well-controlled ability of RAFT polymerization. Therefore, PETD with defined structure and composition was successfully synthesized.

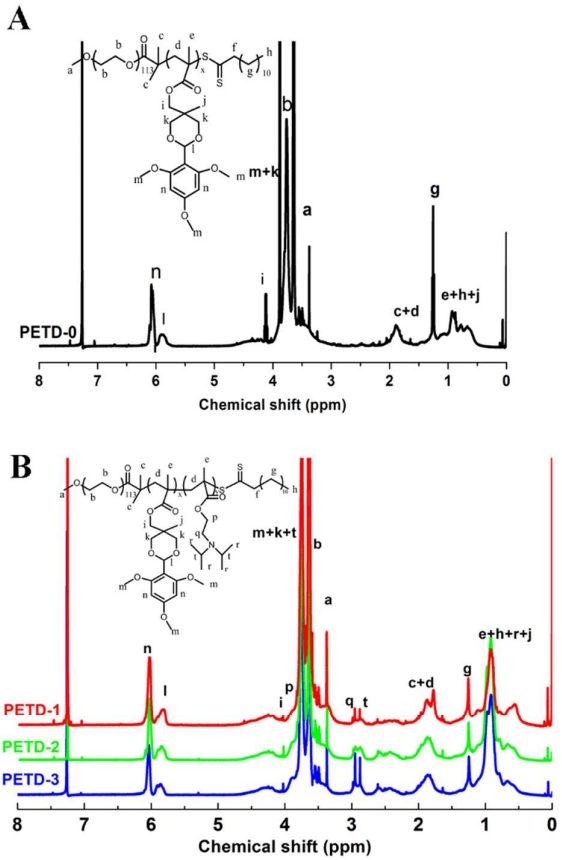

Fig.1 ^{1}H NMR spectra of PETD-0 (A) and PETD-1, PETD-2 and PETD-3 (B) in $CDCl_3$.

Preparation and Characterization of PETD NPs

The CMCs of PETD were measured by pyrene fluorescence probe and the results are shown in Figure S5 and Table S1. The CMCs of all copolymers were only slightly different, ranging from 0.97 mg/L to 0.89 mg/L with increasing the content of DPA segments, which indicated that the incorporated DPA segments had only a slight effect on the CMCs of PETD. The low CMCs may mainly result from high hydrophobicity of aromatic rings.[45] The size distribution and morphology of PETD NPs were investigated by DLS and TEM, respectively. As shown in Figure S6 and Table S1, the mono-disperse NPs with the size ranging from 134.6 to 188.4 nm and polydispersity (PDI) ranging from 0.22 to 0.13 were formed in 10 mM PB (pH 7.4).

Besides, with increasing the content of DPA segments, the size of NPs was an upward trend (Tab. S1), which was probably attributed to the difference of hydrophobicity between DPA and TTMA. The higher DPA content in copolymers could affect the interactions of hydrophobic segments and hence lead to looser and larger aggregates. TEM images (Fig. 2) revealed that PETD could self-assemble into stable NPs with a well-defined spherical morphology and a uniform size distribution ranging from 120 to 170 nm. Meanwhile, TEM results demonstrated that the particle size was increased by increasing DPA content, which was in accordance with the DLS results. The influences

Tab.1 Structure and composition of mPEG-P(TTMA-co-DPA)

Sample	DPA/(TTMA+DPA) (mol/mol)		M_n [b]	M_n [c]	M_w/M_n [c]
	feed[a]	product[b]			
PETD-0	0	0	9983	10249	1.22
PETD-1	0.05	0.058	10007	11074	1.27
PETD-2	0.15	0.13	10189	12358	1.24
PETD-3	0.25	0.24	11030	12069	1.21

[a]Theoretical values.
[b]Calculated from ^{1}H NMR.
[c]Determined by GPC.

of FBS on the stability of PETD NPs were also investigated by DLS and the results were shown in Figure S7. All PETD NPs showed good stability in PBS 7.4 with or without 10% FBS, as there was negligible shift in their size within 72 h.

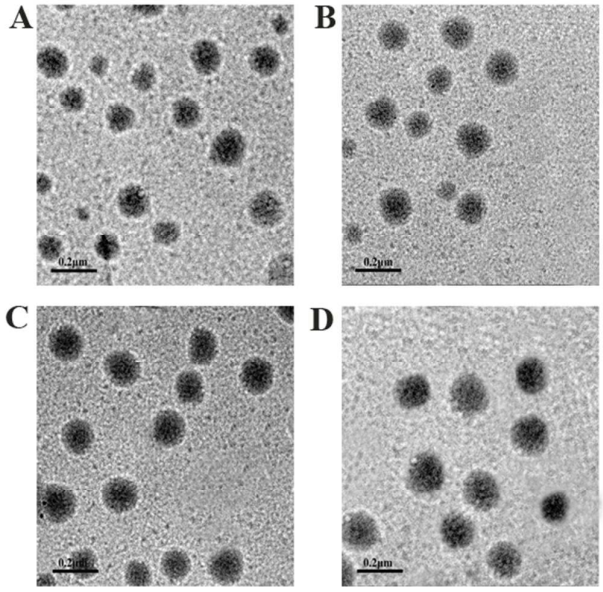

Fig.2 TEM images of PETD-0 (A), PETD-1(B), PETD-2(C) and PETD-3(D) copolymer NPs at pH 7.4.

pH-Dependent Hydrolysis of PETD NPs

It is well known that the degradation or hydrolysis rate of a biodegradable polymer is of great importance for its use in therapeutic applications. The CBAs can be hydrolyzed into polar diol moieties under the physiological acidic pH (4.0–6.5) and change hydrophobic/hydrophilic balance. In order to modulate the hydrolysis rate of TTMA, DPA segments were covalently conjugated into the copolymers. pH-dependent hydrolysis behaviors of the copolymer NPs were determined at

pH of 4.0, 5.0 and 7.4. The hydrolysis degree of nanoparticles was studied by UV/vis spectroscopy by measuring absorbance at 292 nm (Fig.3), which belongs to the characteristic absorbance of hydrolysate (2,4,6-trimethoxybenzaldehyde).[46]

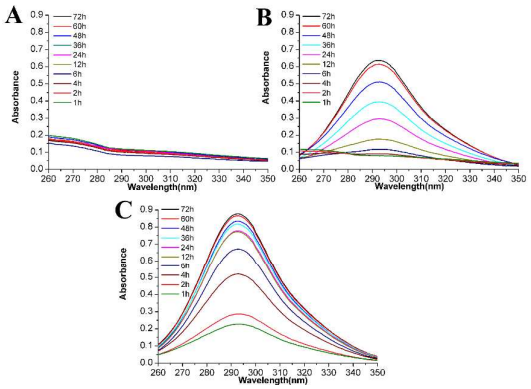

Fig.3 pH-Triggered hydrolysis of acetals in PETD-3 NPs measured by UV/vis spectroscopy at pH 7.4 (A), 5.0 (B) and 4.0 (C).

The hydrolysis kinetic curves shown in Fig. 4 demonstrated that the hydrolysis rate of CBAs in copolymer NPs was highly dependent on acidity of medium. The nanoparticles were relatively stable at pH 7.4, which is consistent with previous reports.[8,26] At the same pH, the hydrolysis rates of acetal followed a general order of PETD-3> PETD-0≈ PETD-2> PETD-1. At pH 7.4, there was little difference in the hydrolysis rates for all nanoparticles, while the difference in the hydrolysis rates became much more pronounced at pH 4.0. It is notable that the hydrolysis of PETD-3 NPs with more DPA was faster than PETD-0 NPs, whereas hydrolysis of PETD-1 NPs is much slower than PETD-0 NPs. At pH 5.0, hydrolysis of PETD-0 NPs was still much faster than that of PETD-1 NPs. Nevertheless, the difference between PETD-3 and PETD-0 samples became less remarkable. This phenomenon could be due to the two opposite effects of PDPA segments on hydrolysis of CBAs.

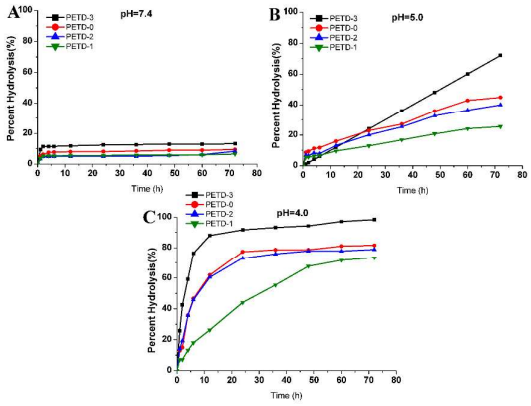

Fig.4 Hydrolysis kinetics of mPEG-b-P (TTMA-co-DPA) at pH 7.4 (A), 5.0 (B) and 4.0 (C).

It has been reported that the hydrolysis rates of acid-sensitive polymers containing CBAs are substantially affected by the hydrophobicity of NPs' core by the decreased local concentration of water and the destabilization of hydrophilic/hydrophobic balance.[47] In this work, we speculated that DPA segments played an amphoteric role in the hydrolysis of acetals, according to the contents of DPA and pH of the medium. On the one hand, the protonation of the tertiary amine of DPA in acidic medium lead to an enhanced uptake of water molecules and hydroniums in the hydrophobic microdomains of the NPs, which expedited the hydrolysis of acetals. On the other hand, the hydronium was consumed during the protonation of the tertiary amine known as buffering effect, which caused transient rise of the local pH in the microenvironment around the tertiary amine units and decreased the hydrolysis rate of acetals. In the case of PETD-3 with sufficient tertiary amine unites, the hydrophilicity increase caused by the protonation can quickly counter balance the consumption of hydroniums, while for PETD-1, the buffering effect plays a dominating role which hindered the hydrolysis of acetal. Therefore, these two opposite impacts function in different ways, conducing to various hydrolytic degradation behaviors of PETD NPs.

Hydrophobic segments of PETD containing the CBAs groups can be partially hydrolyzed into a hydrophilic backbone in the acidic medium. The transition from hydrophobicity to hydrophilicity caused by acid can induce the morphological changes of the nanostructure. The size changes of the NPs caused by acetal hydrolysis at acidic pH were monitored by DLS measurements. As shown in Fig. 5, the sizes of PETD-3 NPs were increased from 188 nm to about 300 nm in 12 h and to over 800 nm in 24 h at pH 5.0 acetate buffer (10 mM). This swelling and aggregation of nanopartilces was ascribed to the enhanced hydrophilicity of micellar core due to acetal hydrolysis. Moreover, a large amount of small-sized particles (about 8 nm) were detected within 60 h incubation at pH 5.0, which elucidated that PETD-3 NPs were completely disassembled and degraded into hydrophilic unimers as we previously reported.[48] In addition, there was no distinguishable difference between the NPs sizes within 24 h at pH 7.4 (data not shown), which suggested the superior colloidal stability of the NPs under physiological conditions.

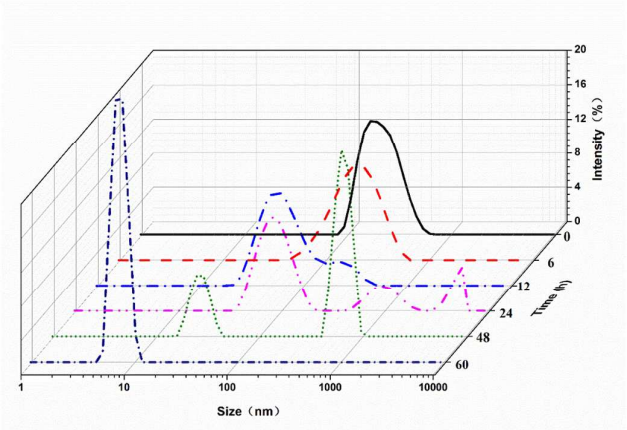

Fig. 5 pH-induced size changes of PETD-3 NPs at pH5.0

Drug-loading and *in Vitro* pH-Triggered Release of DOX

As mentioned above, a well-designed polymeric nanocarrier should hold a high drug loading capacity and be stable in physiological conditions before accumulation into the pathologic area. DOX, which is a prominent anticancer drug for clinical applications, was encapsulated into the NPs to evaluate the loading and release kinetics of PETD NPs. The theoretical DLC was set as 5, 10 and 20 wt%. As shown in Table 2, all four samples exhibited considerably high DLE, which was presumably caused by the strong π–π conjugate interaction between PTTMA and DOX. Notably, DLE decreased with increasing theoretical DLC. Taking PETD-3 NPs for example, DLE decreased from 76.2% to 56.3% when increasing theoretical DLC from 5 wt% to 20 wt%. It should be further noted that at similar drug loading levels, DLE decreased with increasing the content of DPA, which may be attributed to the weakened π-π stacking caused by the addition of DPA. It can be also seen that, the average diameters of DOX-loaded NPs were decreased at a low DLC while the particle diameters became larger with further increasing of DLC. For example, the average size of PETD-3 NPs was decreased from 188.4 nm to 175.2 nm at DLC of 4.2 wt%, and then increased to 208.1 nm and 217.0 nm when further increasing DLC to 7.02 wt% and 10.78 wt%, respectively.

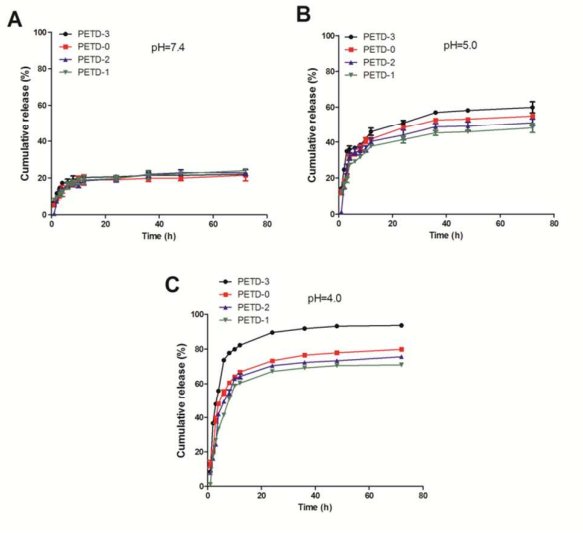

Fig.6 pH-dependent release of DOX from PETD NPs with DLC of 5 wt% at 37°C at pH 7.4 (A), 5.0 (B) and 4.0 (C), respectively.

Tab. 2 Characteristics of DOX-Loaded mPEG-P(TTMA-co-DPA) NPs in PBS 7.4

Sample	Theoretical DLC (%)	DLC(%)[a]	DLE (%)	size (nm)[b]	PDI[b]
PETD-0	5	4.20±0.02	84.0±0.5	125.7±0.3	0.16±0.01
	10	7.92±0.11	79.2±1.5	138.6±3.2	0.18±0.02
	20	13.01±0.32	65.1±1.9	155.7±0.1	0.19±0.01
PETD-1	5	4.07±0.05	81.4±1.0	140.6±1.0	0.21±0.02
	10	7.62±0.21	76.2±2.5	158.1±4.9	0.20±0.02
	20	12.48±0.33	62.4±1.7	171.7±1.9	0.22±0.03
PETD-2	5	3.81±0.06	76.2±1.2	164.0±2.3	0.19±0.02
	10	7.21±0.22	72.1±1.3	182.2±3.5	0.20±0.05
	20	11.25±0.41	56.3±2.1	191.8±2.6	0.22±0.09
PETD-3	5	3.65±0.08	73.0±1.4	175.2±4.2	0.17±0.03
	10	7.02±0.16	70.2±1.8	208.1±3.8	0.19±0.07
	20	10.78±0.37	53.9±2.0	217.0±6.3	0.23±0.04

[a]Evaluated by UV/vis measurements.
[b]Measured by DLS at a concentration of 1.0 mg/mL.

The *in vitro* release of DOX from PETD NPs with DLC of 5 wt% was conducted at 37 °C at pH 7.4, 5.0 and 4.0 and the results were shown in Figure 6. The release of DOX from all four copolymer NPs was much faster at acidic pH (5.0 and 4.0) compared to physiological pH (7.4). For instance, only 20.7% of DOX was released from DOX-loaded PETD-3 NPs within 24 h at pH 7.4, whereas 44.4% and 73.8% of DOX were released in 6 h at pH 5.0 and 4.0, respectively. The obvious increase in DOX release under acidic condition can be ascribed to the swelling and disassembly of the NPs caused by the pH-triggered CBAs hydrolysis. It can be noted from Fig. 6 that at the same pH, the drug release rate also follows the order of PETD-3> PETD-0≈ PETD-2> PETD-1 which is in concordance with the CBAs hydrolysis results. Approximately 73.8%, 55.0%, 49.3%, and 41.5% of DOX was released in 6 h at pH 4.0 from PETD-3, PETD-0, PETD-2 and PETD-1 NPs, respectively. This can be attributed to the bidirectional function of DPA segments in CBAs hydrolysis. At pH 5.0, the differences in the rates of drug release between PETD-3 and PETD-0 samples became slightly decreased compared with pH 4.0.

With the protonation of the DPA segments in PETD-3 NPs, a great quantity of interconnected hydrophilic channels or pore canals were formed, which stimulated the release rate of DOX. However, in PETD-1 NPs, the buffering effect of DPA played a dominating role and less amounts of hydrophilic channels were generated, which led to even slower release rate of DOX than that of PETD-0. The accelerating function caused by DPA protonation at pH 5.0 was less remarkable than that at pH 4.0 because the protonation extent of DPA units is much lower at pH 5.0. At neutral buffer pH 7.4, DPA units are little protonated because the pH value was higher than the pKa value (6.4) of DPA. Thus, DPA units exert little effect on the release of DOX. PETD-3 NPs which are expeditiously responsive to mild acid pH and capable of simultaneous release of hydrophobic drugs, are particularly appealing in cancer therapy.

***In vitro* cytotoxicity assay**

In order to investigate the biocompatibility of PETD NPs, the cell viability was determined by MTT toward HepG-2 cells with

a concentration of 1.0 mg/mL and the results are displayed in Fig. 7. As shown in Fig. 7A, PETD NPs were practically non-toxic (cell viabilities≥92%) at all tested concentrations which confirmed their excellent compatibility. Anticancer efficiency of the DOX-loaded PETD NPs were evaluated in HepG-2 cells using MTT assay. HepG-2 cells were treated for 48 h with free DOX and DOX-loaded PETD NPs. It can be seen from Fig. 7B that all three DOX-loaded NPs displayed a dosage-dependent cytotoxicity, demonstrating that the drug-loaded PETD NPs are able to kill cancer cells. Meanwhile, the drug has been efficiently delivered and released in HepG-2 cells. Interestingly, the results in Fig. 8B displayed that PETD-3 NPs had a low IC_{50} (*in vitro* half maximal inhibitory concentration) value of 0.96 μg/mL for HepG-2 cells, which was relatively close to that of free DOX (IC_{50} =0.30 μg/mL for HepG-2). By contrast, PETD-0 and PETD-1 NPs showed relatively lower inhibition efficiency compared with PETD-3, which illustrated that the faster DOX release from DOX-loaded PETD-3 NPs triggered by endo/lysosomal pH played a significant role in enhancing the anticancer cell proliferation.

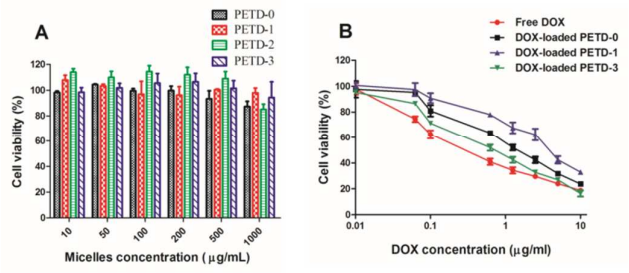

Fig.7 Viability of HepG2 cells after incubation for 48 h with PETD NPs at various concentrations (A). Viability of HepG2 cells after being incubated with free DOX, DOX-loaded PETD NPs for 48 h (B).

In vitro Cell Uptake

The cellular uptakes and pH-triggered intracellular release of DOX were observed in HepG-2 cells by the use of fluorescence microscopy as DOX exhibits red fluorescence. The cells treated by free DOX were used as the control. As expected, strong intracellular fluorescence appeared in the cytoplasm and nucleus of cells after 2 h of incubation with the DOX-loaded PETD-3 NPs (Fig. S8). The DOX fluorescence became even stronger in the cell nuclei at a longer incubation time of 4 h as shown in fig. 8, which was quite similar to that detected for HepG-2 cells following 4 h incubation with free DOX. The relatively weaker DOX fluorescence was found mainly in the cytoplasm of the cells which were incubated with the DOX-loaded PETD-0 NPs. By contrast, the weakest fluorescence was found in the cytoplasm of cells treated by PETD-1 NPs. These intracellular drug release observations were inline with higher anti-tumor activity as well as the more expeditious drug release of DOX-loaded PETD-3 NPs as compared to PETD-0 and PETD-1 NPs. To qualify the amount of DOX delivered in the cells, the mean fluorescence intensity was evaluated by flow cytometry. As shown in Fig. 9, stronger fluorescence intensity was detected in HepG-2 cells after incubated with DOX loaded PETD-3 NPs for 2h and 4h. These results indicated that the PETD-3 NPs with pH-sensitive cyclic benzylidene acetals held hold great potential as carrier for intracellular DOX delivery *via* rapid responsiveness to the low endo/lysosomal pH with relative high drug loading capacity.

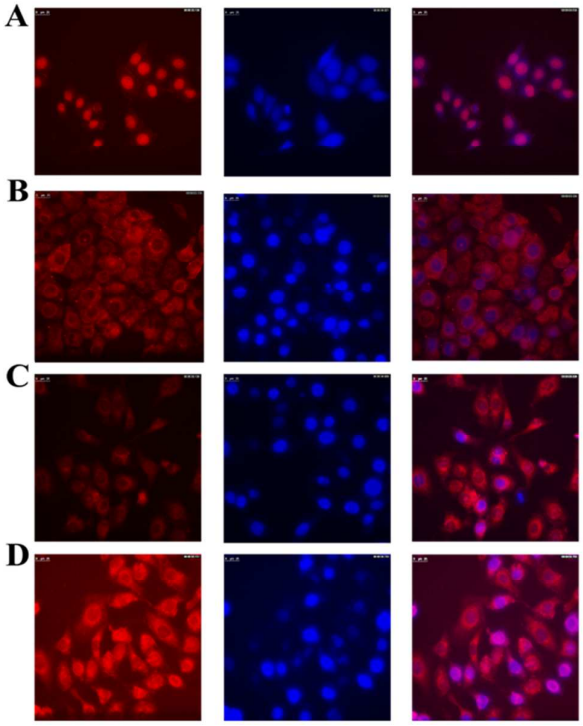

Fig.8 Fluorescence microscopy images of HepG-2 cells following 4 h incubation with DOX-loaded NPs and free DOX (30μg/mL). (A) Free DOX, (B) DOX-loaded PETD-0 NPs, (C) DOX-loaded PETD-1 NPs and (D) DOX-loaded PETD-3 NPs. For each panel, the images from left to right showed DOX fluorescence in cells (red), cell nuclei stained by DAPI (blue), and overlays of both images.

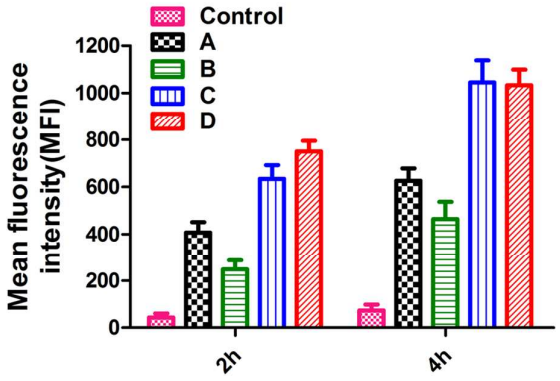

Fig.9 Mean fluorescence intensity on HepG-2 cells after treatment with (A) DOX-loaded PETD-0 NPs, (B) DOX-loaded PETD-1 NPs and (C) DOX-loaded PETD-3 NPs and(D) Free DOX at different incubation time measured by flow cytometry.

Conclusions

PETD bearing TTMA units and DPA units with different feed ratios were successfully synthesized. PDPA segments function

in two opposite but competitive ways in the hydrolysis rate of the CBAs groups, in which buffering effect decreases the hydrolysis rate with a low DPA content (5.8%) while protonation-enhanced hydrophilicity facilitates the hydrolysis with a higher DPA content (24.0%). Due to the hydrolysis of CBAs around mild acid condition, PETD NPs could go through swelling and disassembly, which in turn results in drug release following almost the same order of hydrolysis. Besides, the cell uptake and *in vitro* cytotoxicity assay indicate that more DOX is released into the nucleic of HepG-2 cells treated with DOX-loaded PETD-3 NPs. In summary, this work provides a promising method to modulate the hydrolysis of the CBAs-containing polymers by covalently conjugating different contents of DPA segments for smart carrier designing and clinic therapy while PETD-3 NPs hold great potential in intracellular anticancer drug delivery.

Acknowledgements

This work was supported by a grant from the National Natural Science Foundation of China (Number 81371667, 81471727) and the Specialized Research Fund for the Doctoral Program of Higher Education (20120032110013)

Notes and references

1. Kumar S, Dory YL, Lepage M, Zhao Y. 2011. Macromolecules 44:7385-93
2. Xiao X, He S, Dan M, Huo F, Zhang W. 2014. Chemical Communications 50:3969-72
3. VanBlarcom DS, Peppas NA. 2011. Biomedical Microdevices 13:829-36
4. Araujo JV, Davidenko N, Danner M, Cameron RE, Best SM. 2014. Journal of Biomedical Materials Research Part A: n/a-n/a
5. Ling D, Park W, Park S-j, Lu Y, Kim KS, et al. 2014. Journal of the American Chemical Society 136:5647-55
6. Gillies ER, Frechet JMJ. 2003. Chemical Communications: 1640-1
7.Sonaje K, Lin K-J, Wang J-J, Mi F-L, Chen C-T, et al. 2010. Advanced Functional Materials 20:3695-700
8. Meng F, Zhong Z, Feijen J. 2009. Biomacromolecules 10:197-209
9. Upadhyay KK, Bhatt AN, Mishra AK, Dwarakanath BS, Jain S, et al. 2010. Biomaterials 31:2882-92
10. Xing L, Zheng H, Cao Y, Che S. 2012. Advanced Materials 24:6433-7
11. Dai S, Ravi P, Tam KC. 2008. Soft Matter 4:435-49
12. Sideratou Z, Tsiourvas D, Paleos CM. 2000. Langmuir 16:1766-9
13. Kozlovskaya V, Kharlampieva E, Drachuk I, Cheng D, Tsukruk VV. 2010. Soft Matter 6:3596-608
14. Binauld S, Stenzel MH. 2013. Chemical Communications 49:2082-102
15. Griset AP, Walpole J, Liu R, Gaffey A, Colson YL, Grinstaff MW. 2009. Journal of the American Chemical Society 131:2469
16. Huh KM, Kang HC, Lee YJ, Bae YH. 2012. Macromolecular Research 20:224-33
17. Lee ES, Gao Z, Bae YH. 2008. Journal of Controlled Release 132:164-70
18. Helmlinger G, Schell A, Dellian M, Forbes NS, Jain RK. 2002. Clinical Cancer Research 8:1284-91
19. Sawant RM, Hurley JP, Salmaso S, Kale A, Tolcheva E, et al. 2006. Bioconjugate Chem. 17:943-9
20. Chen H, Zhang H, Thor D, Rahimian R, Guo X. 2012. European Journal of Medicinal Chemistry 52:159-72
21. Tang R, Ji W, Panus D, Palumbo RN, Wang C. 2011. Journal of Controlled Release 151:18-27
22. Hrubý M, Koňák Č, Ulbrich K. 2005. Journal of Controlled Release 103:137-48
23. Jin Y, Song L, Su Y, Zhu L, Pang Y, et al. 2011. Biomacromolecules 12:3460-8
24. Yoo HS, Lee EA, Park TG. 2002. Journal of Controlled Release 82:17-27
25. Du Y, Chen W, Zheng M, Meng F, Zhong Z. 2012. Biomaterials 33:7291-9
26. Chen W, Meng F, Li F, Ji S-J, Zhong Z. 2009. Biomacromolecules 10:1727-35
27. Miao K, Shao W, Liu H, Zhao Y. 2014. Polymer Chemistry 5:1191-201
28. Hu YQ, Kim MS, Kim BS, Lee DS. 2007. Polymer 48:3437-43
29. Soppimath KS, Aminabhavi TM, Kulkarni AR, Rudzinski WE. 2001. Journal of Controlled Release 70:1-20
30. Brannon-Peppas L, Blanchette JO. 2004. Adv. Drug Deliv. Rev. 56:1649-59
31. Petros RA, DeSimone JM. 2010. Nat. Rev. Drug Discov. 9:615-27
32.Du J-Z, Mao C-Q, Yuan Y-Y, Yang X-Z, Wang J. 2014. Biotechnology Advances32:789-803
33.Wilhelm M, Zhao CL, Wang Y, Xu R, Winnik MA, Mura JL. 2009. Journal of the American Chemical Society 131:2469-2471
34. Griset AP, Walpole J, Liu R, Gaffey A, Colson YL, Grinstaff MW. 2009. Journal of the American Chemical Society 131:2469
35. Chen W, Zhong P, Meng F, Cheng R, Deng C, et al. 2013. Journal of controlled release: official journal of the Controlled Release Society 169:171-9
36. Zubris KA, Liu R, Colby A, Schulz MD, Colson YL, Grinstaff MW. 2013. Biomacromolecules 14:2074-82
37. Junqiang Zhao, Jinjian Liu, Shuxin Xu, et al. 2013. ACS Appl. Mater. Interfaces 5(24):13216-13226
38. Thomas HF, Jao LK.1964The Journal of Organic Chemistry. 30:1492-95
39. Oshima T, Ueno SY, Nagai T. 1995. Heterocycles 40:607-17
40. Pluth MD, Bergman RG, Raymond KN. 2009. J. Org. Chem. 74:58-63
41. Dayananda K, Kim MS, Kim BS, Lee DS. 2007. Macromolecular Research 15:385-91
42. Du JZ, Fan L, Liu QM. 2012. Macromolecules 45:8275-83
43. Pearson RT, Warren NJ, Lewis AL, Armes SP, Battaglia G. 2013. Macromolecules 46:1400-7
44. Moad G, Chong YK, Postma A, Rizzardo E, Thang SH. 2005. Polymer 46:8458-68
45. Ma YH, Cao T, Webber SE. 1998. Macromolecules 31:1773-8
46. Wu Y, Chen W, Meng F, Wang Z, Cheng R, et al. 2012. Journal of Controlled Release 164:338-45
47. Gillies ER, Jonsson TB, Frechet JMJ. 2004. Journal of the American Chemical Society 126:11936-43
48. Zhao J, Wang H, Liu J, Deng L, Liu J, et al. 2013. Biomacromolecules 14:3973-84

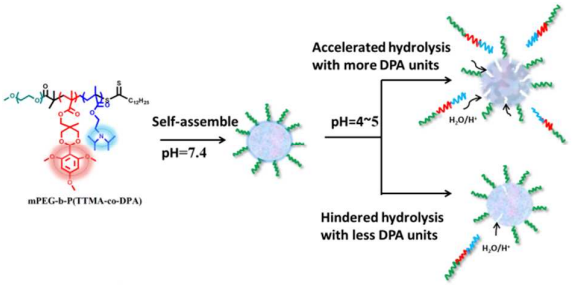

Introduction of DPA units into PECD copolymer have an amphoteric effect on the hydrolysis behavior of CBAs under acid conditions.